THE EFFECTS OF HEAT TREATMENT ON 7075 Al COLD SPRAY DEPOSITS

M.R. Rokni[a], C.A. Widener[b], V.K. Champagne[c], G.A. Crawford[b], S.R. Nutt[a]

[a] M.C. Gill Composites Center, Department of Chemical Engineering and Materials Science, University of Southern California, Los Angeles, CA, USA.
[b] Department of Materials & Metallurgical Engineering, Advanced Materials Processing Center, South Dakota School of Mines & Technology (SDSM&T), Rapid City, SD, USA.
[c] U.S. Army Research Laboratory, Weapons and Materials Research Directorate, Aberdeen Proving Ground, Maryland, USA.

ABSTRACT: High-pressure cold spray was used to deposit 7075 aluminum powder onto 7075-T6 substrates. We investigated the effects of post deposition heat treatments on the microstructure and mechanical properties of the deposits. For this purpose, both low-temperature and high-temperature treatments were carried out on specimens excised from the deposits. Microstructures of the as-deposited and heat treated samples were characterized via different microscopy techniques and mechanical properties were evaluated by microtensile and hardness tests. The results were then correlated with the observed microstructures in different conditions. The strength and ductility of the cold sprayed 7075 deposits increased after both low- and high-temperature treatments, which resulted in precipitation of strengthening phases and increased inter-particle bonding. Because of a change in bonding mechanism, heat treatment at high temperature yielded markedly greater ductility than all other conditions. Diffusion and microstructural sintering at the particle-particle interfaces were proposed to cause the change in bonding mechanism from mechanical interlocking to metallurgical bonding and lead to the ductile characteristics of these samples. The understanding gained from this research should lead to optimization of and pre- and post processing treatments for cold spray deposits.

1. INTRODUCTION

Cold spray (CS) has gained traction as a repair process, especially for components of military systems, where replacement costs and downtime are prohibitively high and long. Ideally, repaired parts should exhibit mechanical properties equivalent to or superior to the parent materials. However, while CS deposits generally show high strength because of the severe plastic deformation (SPD) intrinsic to CS, they often exhibit decreased ductility because of the extensive cold work and/or porosity in the deposit [1-4]. Effort has been made to improve the quality of the CS deposits by reducing porosity and thereby achieve superior combinations of ductility and strength [3-7].

High-pressure cold spray (HPCS) systems can address this problem by producing deposits with reduced porosity and improved ductility [2-8]. In addition to reducing porosity, HPCS also produces more extensive deformation compared with low-pressure systems, giving rise to ultra-fine grain (UFG) structures, particularly at prior particle boundaries (PPBs) [4, 5, 10-13]. According to the literature on various SPD processes [13-17], development of these UFG structures can also enhance the mechanical properties, e.g. strength, hardness and ductility, of the processed materials.

The strength of CS deposits can also be increased by introducing small precipitates through performing heat treatment (HT) in age hardenable alloys, such as 2xxx, 6xxx, and 7xxx Al [18-25]. This is because deformation prior to HT is commonly used to foster heterogeneous nucleation of precipitates in these alloys. This approach has been reported for 7xxx Al alloys after processing

by SPD techniques [21-25]. One study on CS 7075 deposits [6] showed that deposits were strengthened by aging, yielding an increase of ~ 60 HV hardness after T73 heat treatment. Because CS is a relatively new SPD process used primarily for repairs, the effects of HTs on strength and ductility of the deposits warrants investigation.

High-temperature HTs of CS deposits, including annealing and solutionizing, reportedly increase the ductility, albeit at the expense of strength, which often decreases [26-32] because of grain growth. However, *in situ* microstructural observations have shown that solute segregation to grain boundaries (GBs) during heat treatment can stabilize UFG structures against grain growth [9, 13, 32]. In the present study, we also investigate on the effects of high temperature HTs on structure and mechanical properties of CS 7075 deposits.

CS is an SPD process, but compared with conventional wrought alloys that are sometimes stretched prior to aging, the deformation microstructure in CS deposits is much less homogeneous [2-4]. Thus, designing and optimizing a single HT for CS deposits may not be possible, and evaluating conventional HT's provides a useful starting point.

The present research was initiated to investigate the effect of both low- and high-temperature HTs on the structure and mechanical properties of CS 7075 Al, including strength, ductility, and hardness. The results are compared and contrasted with the properties of the as-deposited (AD) and bulk alloys. The 7075 Al alloy an age-hardenable alloy that is widely used for structural components in military and civilian aircraft, as well as in the automotive industry [32-34]. However, there have been no reports of the effects of HTs on the strength and ductility of CS deposits of 7075 Al. In this work, we report measured mechanical properties and correlate the values to corresponding microstructures after heat treatment using microscopy techniques. The

fracture surfaces were also analyzed to assess bonding mechanisms in AD and HTed materials. Note that ductility is used as a critical performance metric for repairs implemented by CS, partly because ductility is readily measured. Also, ductility can contribute to fracture toughness, which is more difficult to measure, particularly for coatings.

2. EXPERIMENTAL PROCEDURE

2.1. COATING PREPARATION

7075 Al coatings were produced using gas-atomized 7075 Al powder (Valimet, Stockton, CA, USA), 18.6 ± 8.2 µm in size. Feedstock powder size was measured using a laser diffraction particle size analyzer (S3000, Microtrac, Montgomeryville, PA). Helium process gas was used to achieve high impact velocities. The deposits were produced using a high-pressure cold spray system (VRC Gen III, VRC Metal Systems, Rapid City, SD, USA) and the pressure and temperature of helium were maintained at 2.8 MPa and 400˚C at the heater exit, respectively. Deposition was performed using a nozzle stand-off distance of 25 mm, 90° deposition angle, medium powder feed rate (12 g min^{-1}), and a nozzle traveling speed of 600 mm s^{-1}, yielding a total deposition thickness of ~ 8.5 mm.
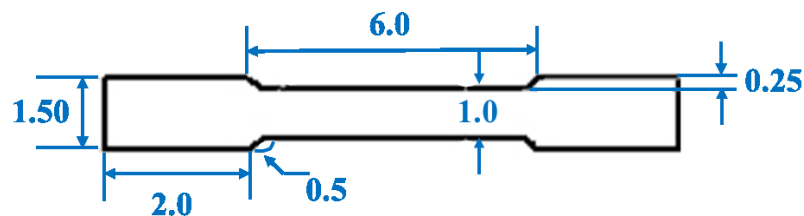

Fig. 1. Specimen geometry used for microtensile testing. All dimensions are in mm.

2.2. MICROTENSILE SAMPLES

Uniaxial tensile testing was carried out at room temperature with a loading rate of 200 µm/min in a universal testing machine (MTS 810, MTS Systems Corporation, Minneapolis, MN, USA). Tensile testing coupons were machined from the as-deposited cold spray samples with the dimensions shown in Fig. 1. These specimens were fine polished on both sides to remove/minimize surface defects, resulting in a final thickness of 1.0 mm. Specimens were machined such that the tensile axis was perpendicular to the spray direction. A total of 12 samples were tested, including three samples for each of the following conditions: as-deposited, stress relieved, T6 aged, and substrate material (bulk).

2.3. HEAT TREATMENTS (HTs)

Six HTs were performed on as-deposited CS samples, including as-deposited (AD, no heat treatment), T6, solution treating + T6 (ST+T6), stress relief (SR), T7X, T73, as well as annealing treatments. These HTs are commonly used for 7075 Al alloys, and are summarized in Table 1. Note that the time and temperature used for all HTs were the same as those used for conventional HTs, although they are likely to be different for SPD alloys, i.e. CS deposits. All HTs were performed in an open air furnace (Lindberg 51894, Riverside, MI), and the 7075 Al substrate material was received in T6 condition.

Table 1. Time and temperature conditions for the applied heat treatments [35].

Condition	Temperature (°C)	Time
AD	RT	8 months
T6	121	24 h
T73	107 + 163	6 + 24 h

T7X	107 + 163	6 + 4 h
SR	107 + 163	6 + 1 h
Annealing	412	3 h
SS+T6	450 + 121	12 + 24 h

2.4. MICROHARDNESS TESTING

Vicker's microhardness measurements were performed on the CS 7075 Al material in as-deposited and heat-treated conditions, as well as on the bulk 7075-T6 material using a Vicker's microhardness tester (HMV-2, Shimadzu, Tokyo, Japan) and an indenter load of 300 g. For all the microhardness values reported, 15 measurements were performed, and the standard deviations were calculated.

2.5. MICROSTRUCTURE CHARACTERIZATION

The microstructure of the as-received powder and CS deposits were characterized using transmission and scanning electron microscopy (TEM and SEM), as well as electron back-scattered diffraction (EBSD). TEM micrographs were obtained at 200 kV (JEM-2100, JEOL Ltd., Tokyo, Japan). Thin discs, 3 mm in diameter, were excised from the deposits, then polished, dimpled, and ion milled for 4 hours. SEM and EBSD analyses of the as-received powders and cold spray deposits were conducted using a field emission SEM (Supra-40, Zeiss, Oberkochen, Germany) operated at 15 kV. EBSD samples were sectioned from the CSP deposition and

prepared by standard metallographic techniques. Final polish was conducted using 0.05 µm colloidal silica suspension and vibratory polishing.

3. RESULTS AND DISCUSSION

3.1. POWDER CHARACTERIZATION

Figs. 2(a-b) show SEM images of the as-received gas-atomized 7075 Al powder. The particles are spherical with diameter 18.6 ± 4.2 µm. The powder size distribution consists of a mixture of both large (~10-20 µm) and micro-satellite particles (less than 5 µm in size). Fig. 2(b) shows a typical powder particle of ~20 µm, with ~1-4 µm external grain structure. Details of the internal and surface microstructures of the powder particles have been reported [3].
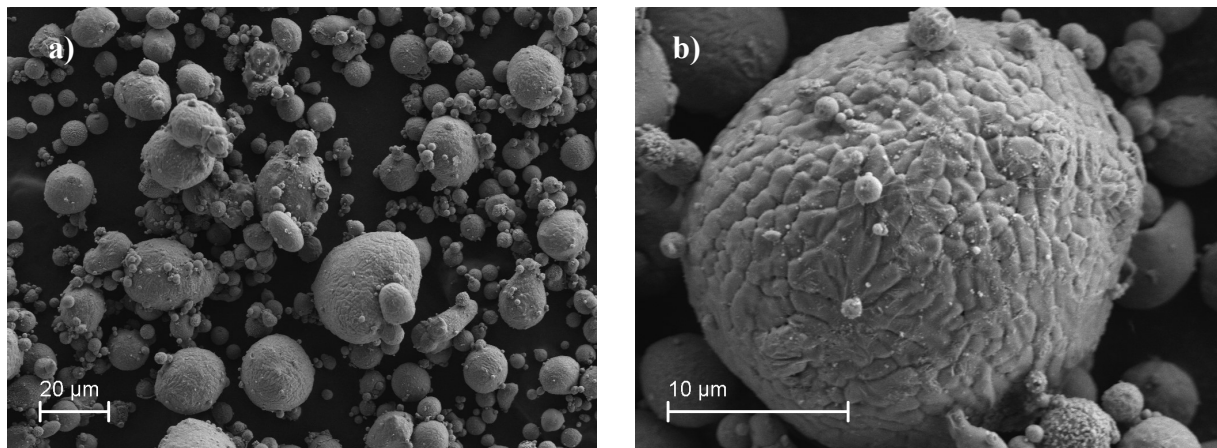

Fig. 2. SEM micrographs of 7075 Al powder showing, a) powder morphology, b) surface structure.

3.2. AS-DEPOSITED MATERIAL

Microstructural characterization of CS deposits prior to ageing was carried out, and Fig. 3 shows typical pattern quality EBSD maps obtained from the CS 7075 Al deposit. Overall, the CS deposit exhibits no evidence of porosity, triple junction voids, or lack of bonding between powder particles. The absence of such defects indicates that the deposition parameters selected resulted in

sufficient particle deformation. Indeed, the originally spherical particles have undergone extensive plastic deformation, as indicated by the dashed lines. The SPD during deposition led to three distinct microstructural regions: 1- particle interior (dashed white line), 2- PPBs with pancake morphology (red arrows) and 3- PPBs with recrystallized UFG structures (white arrows). The curved dark lines in the image correspond to PPBs. The microstructural features in these three regions of the CS 7075 Al deposit have been documented elsewhere [3, 6], although the precipitate morphologies have not.
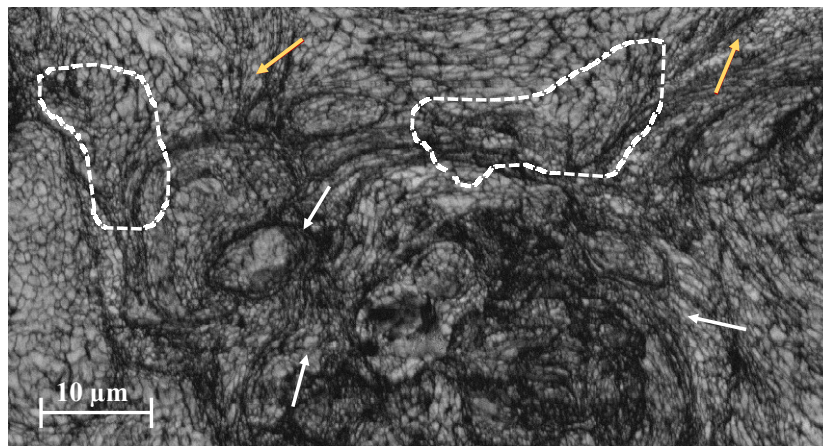

Fig. 3. Pattern quality map from CS 7075 deposit showing different distinct regions in the microstructure; dashed while lines: particle interiors, yellow arrows: PPBs with pancake structure, and white arrows: PPBs with UFG structure.

Fig. 4 shows TEM images of the characteristic regions of the CS 7075 Al deposit. Fig. 4(a) shows the particle interiors, where the microstructure resembles the as-received powder. These regions experience mild deformation during deposition, and exhibit poorly organized dislocation networks and low angle grain boundaries (LAGBs). The particle interiors show little evidence of precipitates.
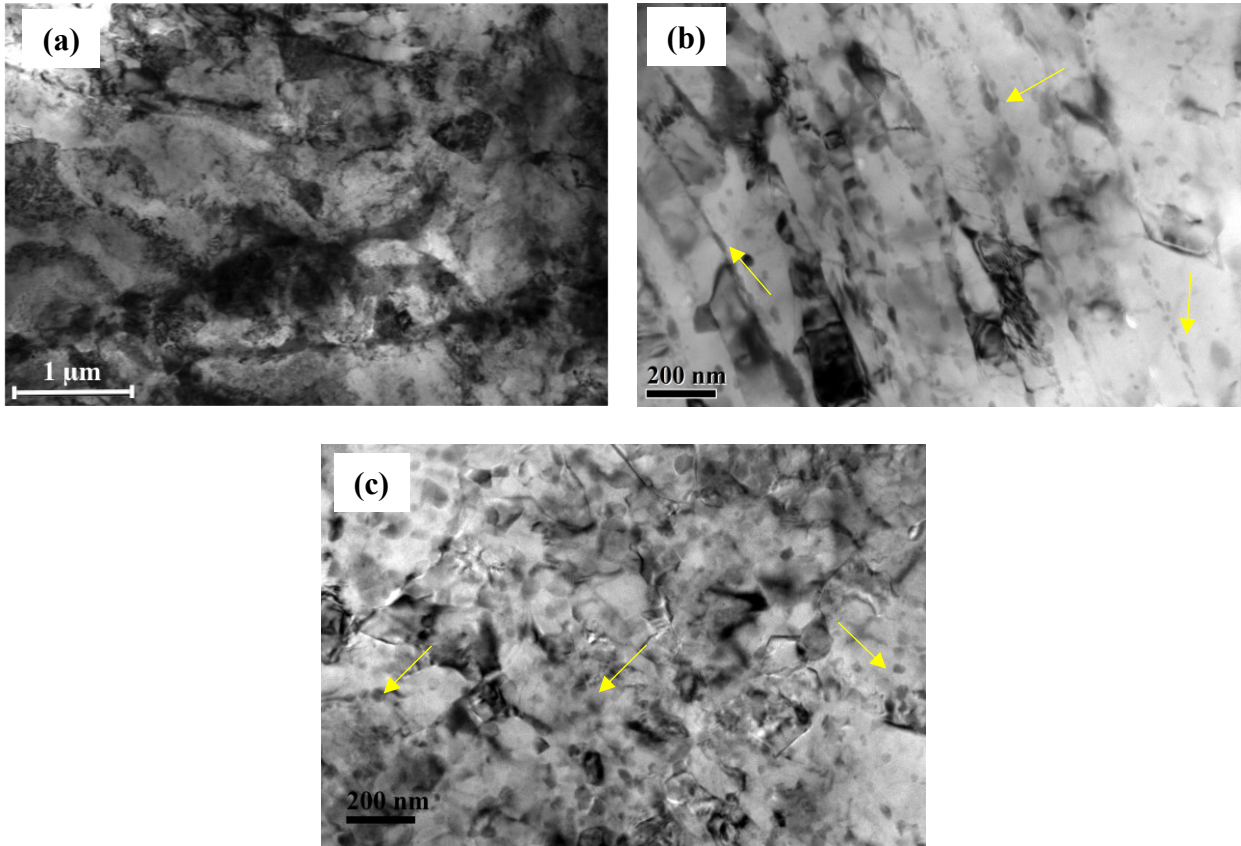
Fig. 4. TEM micrographs from showing precipitate structures in (a) particle interior, (b) PPBs with pancake structures and (c) PPBs with UFG structures of the CS 7075 Al deposit. Yellow arrows in Figs. b & c show needle and spherical precipitates at pancake and UFG regions.

However, Fig. 4(b) shows larger, needle-like precipitates in the pancake grains near PPBs (red arrows), most of which nucleated at high angle GBs (HAGBs). The larger size of these precipitates is attributed to early heterogeneous nucleation, and accelerated growth due to GB diffusion [36, 37]. Fig. 4(c) shows that the UFG structured PPBs contain some spherical and refined precipitates nucleated on both H- and LAGBs (red arrows). The difference in precipitate morphologies between PPBs with UFG and pancake grains is attributed to accelerated aging because of heterogeneous nucleation and more accelerated GB diffusion in the UFG structured regions, which could easily deplete solute within the small grains and inhibit age hardening [36-39].

Fragmentation of precipitates due to the more extensive deformation in the UFG structures produced by CS is another possible reason for the sm all precipitates in these regions.

The XRD pattern from the CS 7075 Al deposit shows extra peaks at ~ 20°, indicated in Fig. 5 by the blue arrow, which belong to newly formed precipitates in the corresponding microstructure. Rokni et al. [32] and Zhau et al. [22] have identified these peaks as η' type precipitates ($MgZn_2$). Because of the high strain levels and temperatures reached during CS, particularly at PPBs [2-7], dynamic and static precipitation, are expected in 7075 Al.
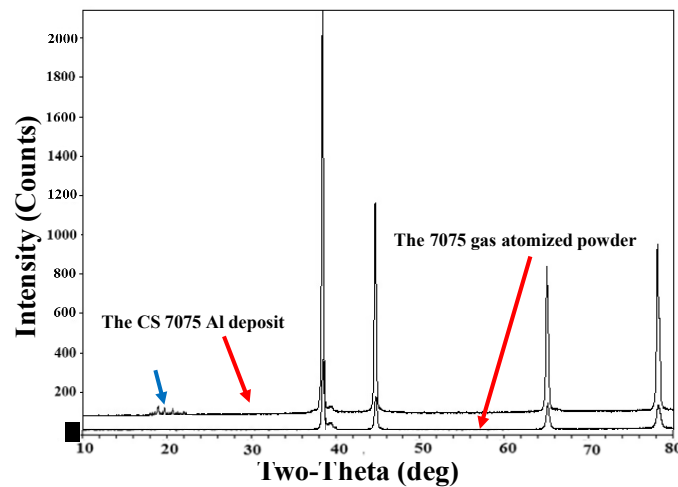

Fig. 5. XRD patterns of the 7075 gas-atomized powder vs. the CS 7075 deposit.

3.3. POST-CS HEAT TREATMENTS

During the CS process, the plastic strain experienced by particles is non-uniform and thus the microstructure of the deposited material is also non-uniform, as discussed in Section 3.2. However, heat treatment (HT) can homogenize the microstructure of CS deposits and generate microstructural features throughout the specimen. Thus, HTs can also be used to enhance and optimize the mechanical properties in CS deposits.

3.3.1. MICROSTRUCTURAL EVOLUTION

Because all low-temperature HTs affected the microstructure of CS 7075 Al deposits similarly, only T6 and T73 treatments are discussed here. Fig. 6(a) shows a Scanning TEM (STEM) micrograph depicting the particle interiors and PPBs in the T6 condition, and enlargements of each region are shown in Fig. 6(b) and 6(c). The dark vein-like features in Fig. 6(a) are GBs and illustrate that the microstructure is heavily precipitated. Both particle interiors and PPB regions are characterized by fine dispersions of the η' transition phase, with diameters of ~ 20 - 60 nm. However, the distribution of the precipitates is different in PPBs and particle interiors. The UFG structures at the PPBs provide abundant GB areas for heterogeneous nucleation of precipitates [19-22]. This leads to a substantially higher number density of the precipitates at the PPBs compared to particle interiors. Comparison of the microstructures of the AD and T6 conditions reveals that recovery has occurred during the T6 treatment, as grain interiors are nearly devoid of dislocations. The microstructure of the CS 7075 Al deposit in the overaged T73 temper is shown in Fig. 7. Over-aging (Table 1) results in growth and coarsening of precipitates in both the particle interiors and the PPBs. As a result, the microstructure in this condition exhibits a coarse but more uniform distribution of precipitates.
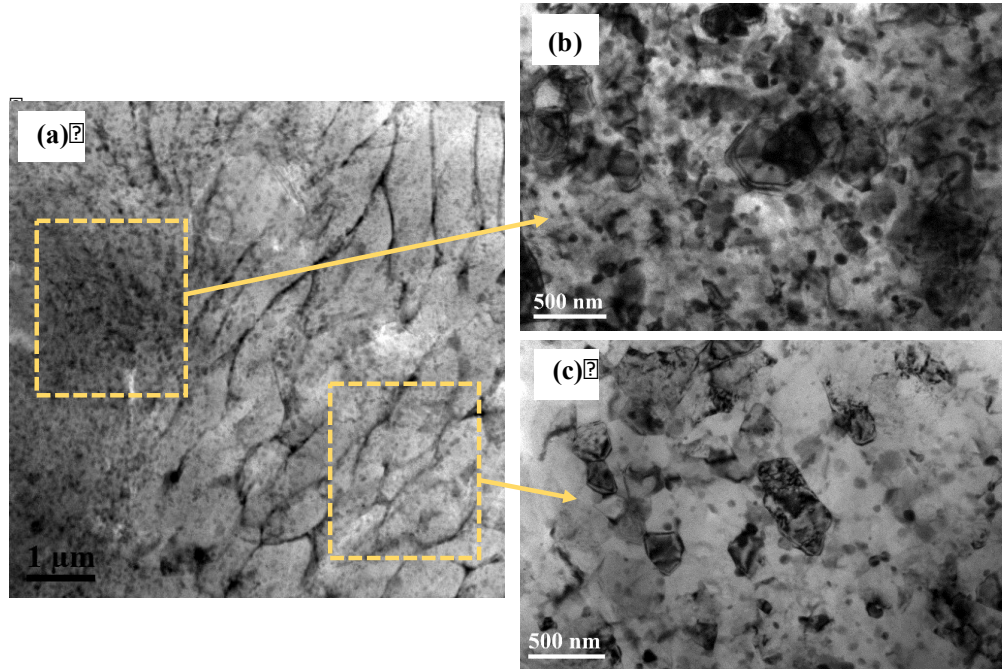
Fig. 6. (a) STEM micrograph of the CS 7075 Al deposit in T6 condition showing distribution of precipitates (b) at the PPBs and (c) in the particle interiors.

TEM micrographs of the annealed CS 7075 Al deposit are shown in Fig. 8. The grains in are typically recrystallized and equiaxed, and the average grain size is $\sim$ 460 nm. The average grain size of UFG structures at the PPBs in different conditions are reported in Table 2. Comparison of the grain size in the AD and annealed conditions reveals that only limited grain growth occurred at the PPBs during annealing. Resistance to grain growth arises from the pinning effect of GB precipitates. However, the annealing process causes the precipitates to grow significantly compared with T6 and T73 conditions. Annealing also produces recrystallized dislocation-free grains, as shown in Fig. 8.
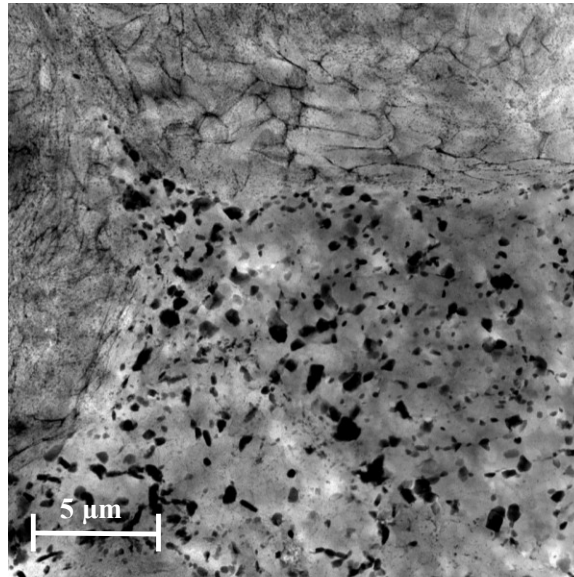
Fig. 7. STEM micrograph of the CS 7075 Al deposit in T73 condition illustrating the presence of larger precipitate size compared to T6 condition.

The microstructure of CS 7075 Al deposits after solutioning and T6 (SS+T6) heat treatment is shown in Fig. 9. Referring to Table 2, grain growth occurs (from 354 ± 47 in AD to 486 ± 19 nm in SS+T6) in the microstructure during the T6 heat treatment. However, Fig. 9 shows that the 12-h solutionizing in this condition provides more homogenous intragranular and transgranular nucleation sites for precipitation during the the subsequent T6 HT.
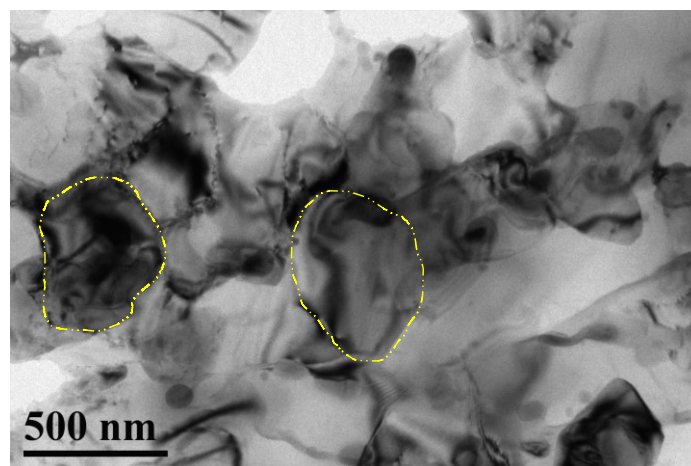

Fig. 8. Microstructure of the CS 7075 Al deposit in annealed condition. The yellow dashed lines trace grain boundaries.

Table 2. The average grain size of UFG structures in the CS 7075 deposit different conditions.

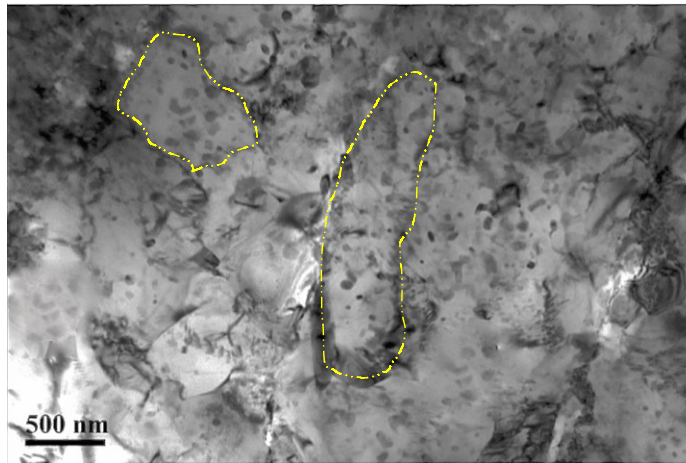| Heat treatment	Grain Size (nm)
AD	354 ± 47
T6	362 ± 39
T73	383 ± 61
T7X	361 ± 42
SR	358 ± 52
Annealed	441 ± 68
SS+T6	486 ± 19

Fig. 9. TEM micrographs of the CS 7075 Al deposit in SS+T6 condition. The yellow dashed lines trace grain boundaries.

3.3.2. TENSILE PROPERTIES AND MICROHARDNESS

The true stress-strain curves for the as-deposited (AD) 7075 material and the six heat treated conditions are shown in Fig. 10. It is seen in Fig. 10 that the AD condition shows the lowest UTS and elongation among all conditions and these properties are remarkably improved through all post-CS heat treatments. Fig. 11 shows the ultimate tensile strength (UTS) and elongation to fracture results for CS 7075 Al samples in all seven conditions. These data were extracted from

the obtained MT test curves, which are illustrated in Fig. 10. The AD 7075 deposit shows the lowest UTS and ductility among all the conditions, a consequence of the extensive cold work introduced into the microstructure during CS. The cold work in the AD material can be understood from the dislocation structures in the microstructure of particle interiors and the UFG structures at the PPBs, shown in Figs. 3 & 4. Interparticle porosity at PPBs in similar CS 7075 deposits has been reported elsewhere [3, 6], causing detrimental effects on tensile properties.
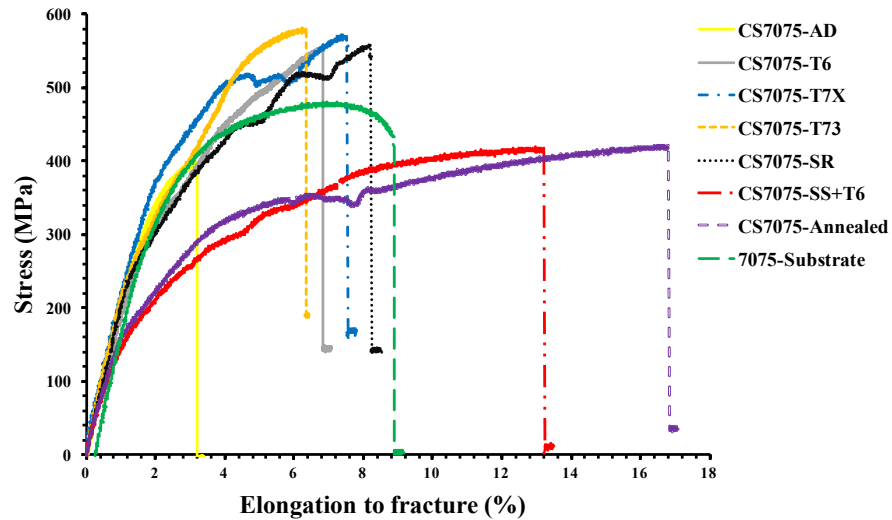

Fig. 10. Stress-strain curves for microtensile specimens of the CS 7075 Al deposit in as-deposited and different heat treatment conditions.

Table 3. The average microhardness of the CS 7075 deposit in different conditions.

Heat treatment	Hardness (Hv)
AD	120 ± 6.1
T6	189 ± 5.6
T73	170 ± 3.4
T7X	164 ± 6.7
SR	159 ± 5.2
Annealed	108 ± 7.4
SS+T6	177 ± 4.0

The mechanical properties of the CS deposit increased after all of the post-CS HTs. Fig. 11 and Table 3 show that low-temperature HTs (T6, T7X, T73 and SR) increase the UTS and ductility of the CS 7075 Al deposit. The increase in the UTS in these conditions occurs as a consequence of precipitation of intermetallic phases, particularly as η' and η (see Figs. 5 & 6). The precipitates impede dislocation movement and thereby increase strength. In all of the low-temperature HT conditions, the hardening effect by aging dominates the softening effects by recovery and as a result, samples heat treated at low temperature are stronger and more ductile. Similar results have been reported for aging of 7075 Al after SPD processing [21].

Heat treatments at higher temperatures (annealing and SS+T6) also improved strength and ductility, as shown in Fig. 11. Similar approaches have been employed to increase the reduced ductility of CS deposits by annealing [27-32]. In most cases, however, anneals led to a decrease in strength due to grain coarsening and relaxation of internal stresses. In contrast, annealing of the CS deposits led to increases in both UTS values and ductility, which increased from ~3.2% in the AD condition to ~14% and 10% in annealed and SS+T6 conditions, respectively (Fig. 11).
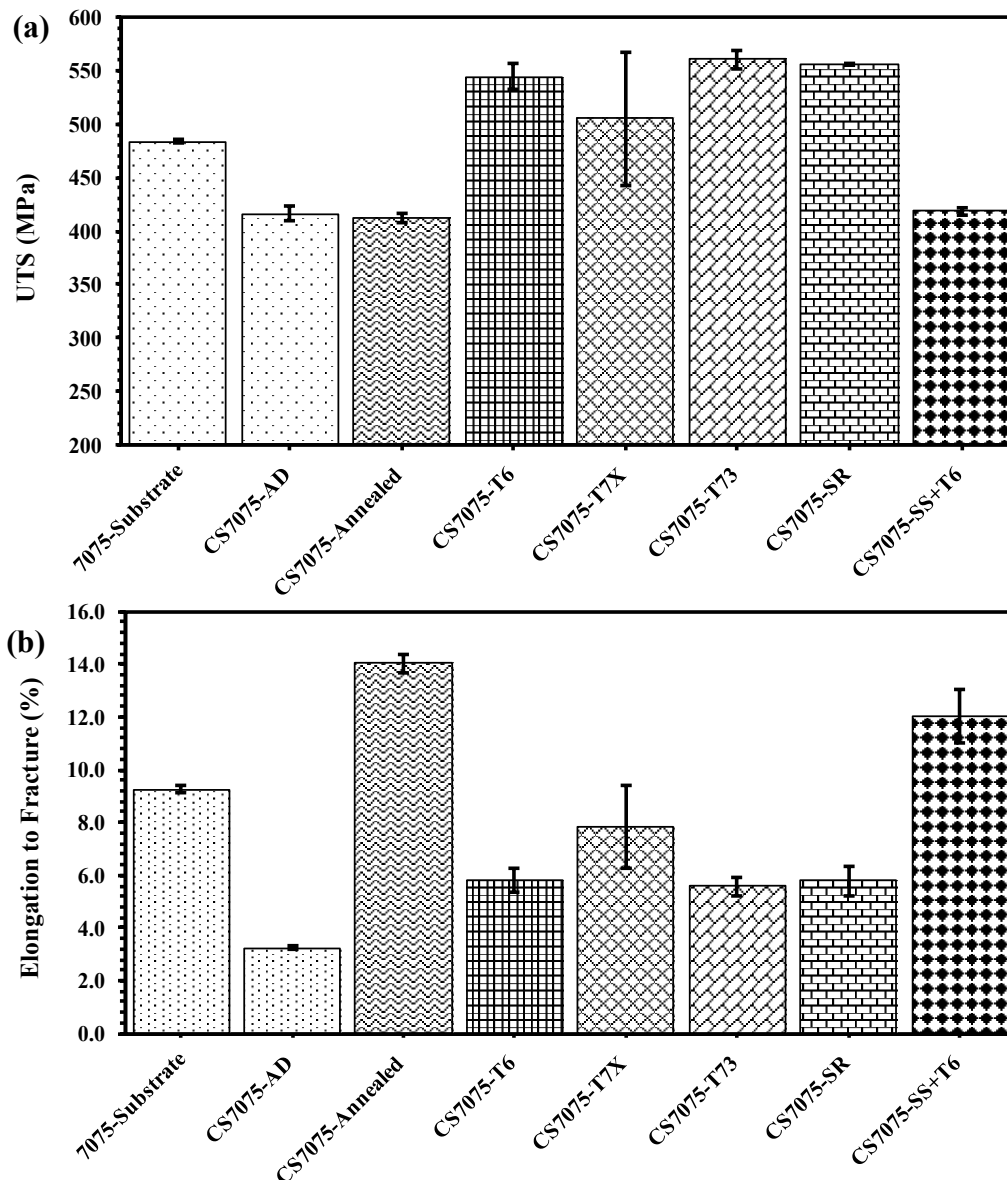
Fig. 11. The (a) UTS and (b) elongation to fracture of microtensile specimens of the CS 7075 Al deposit in as-deposited and different heat treatment conditions. The UTS and elongation of bulk 7075 Al has also been added to the graphs to comparison.

Data in Table 2 show that limited grain growth occurs during annealing, and thus, the UTS of the deposit is unchanged compared to the AD sample. However, in the SS+T6 treatment, grain growth is observed, although the UTS increases from ~ 400 MPa to ~ 425 MPa due to fine distribution of the precipitates that develop [29-31]. Regarding the substantial increase in ductility resulting from

the two high-temperature treatments, this can be attributed to increased metallurgical bonding and fusion at the PPBs [27-32], which is discussed further in the next section.

3.3.3. FRACTOGRAPHY

To more clearly understand deformation mechanisms in the as-sprayed and annealed deposits, fracture surfaces of the tensile samples were analyzed. These two conditions were chosen for analysis because of the difference in elongation (3.2% in AD versus 14% in annealed condition), which might illuminate bonding conditions at PPBs in CS samples.

In the AD sample, shown in Fig. 12(a), the fracture separation occurred primarily at PPBs, and entire particles detached during fracture (indicated by red arrows). The morphology indicated that bonding at PPBs in the as-deposited material relied substantially on mechanical interlocking [27, 29, 31]. However, metallurgical bonding in AD samples cannot be completely ruled out, and PPBs might in fact feature "mixed" bonding – a combination of metallic bonds and mechanical interlocking in indeterminate proportions. This assertion is as yet unproven, and a more thorough investigation is required before reaching definitive conclusions.

Fracture morphology of annealed samples show features distinct from the AD condition, as seen Fig. 12(b). Annealing removes most traces of PPBs on fracture surfaces, which are characterized by dimple arrays that cover both PPBs and particle interiors. These observations indicate that high-temperature treatments of CS deposit alter the bonding mechanism between particles from mechanical interlocking to more metallurgical bonding. This behavior has been reported for other CS materials as well [27-32]. Moreover, the additional sintering that occurs at PPBs in the course

of annealing reduces crack nucleation sites naturally present in the AD materials. The enhanced fusion of particles also contributes to the significant increase in ductility and UTS in almost all HT conditions considered in this study.
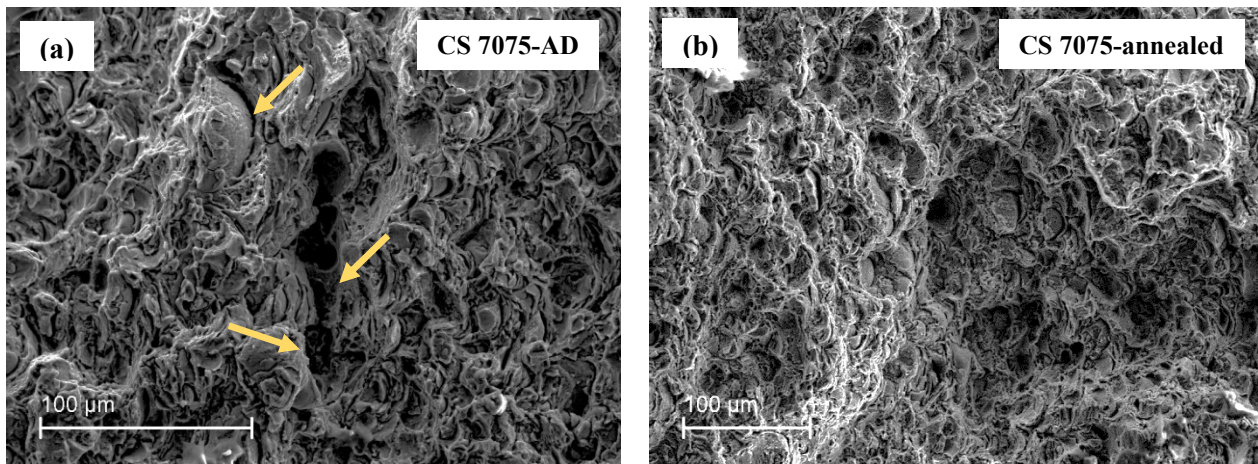

Fig. 12. The fracture surfaces of microtensile specimens of the CS 7075 Al deposit in as-deposited and annealed conditions. The yellow arrows show the location of fracture separation at PPBs.

4. CONCLUSIONS

The objectives of this study were to analyze precipitate morphologies in different regions of the CS 7075 Al deposit and to investigate the effects of conventional HTs on the microstructure and mechanical properties. Microstructural observations of particle interiors showed little evidence of precipitation in these regions. However, pancake structured grains at PPBs showed larger, needle-like precipitates, most of which nucleated at HAGBs. The UFG PPBs contained both spherical and refined precipitates at both H- and LAGBs. The difference in precipitate morphologies between these regions was attributed to more accelerated aging and GB diffusion in the UFG regions.

The microstructure of CS 7075 Al deposits was characterized after low- and high-temperature HTs. The dark vein-like GBs were heavily precipitated after T6 HT. The overaged T73 temper exhibited a coarse but more uniform distribution of precipitates. Annealing CS 7075 Al deposits

produced recrystallized and equiaxed grains. Limited grain growth was observed at PPBs after annealing, but grain was restricted by the pinning effect of GB precipitates. Solutionized+T6 HT produced more homogenous intragranular and transgranular precipitation in the microstructure.

The mechanical properties of the as-deposited material can be increased by conventional low and high temperature HTs used for 7075 Al (stress relief, T7X, T6, and T73). The increases in ductility and strength after low temperature HTs were caused by precipitation of strengthening phases and their hardening effect. Samples heat treated at high temperature (annealed and solutionized + T6), showed slight increases in UTS and markedly increases in ductility. The increase arose from atom diffusion and microstructural sintering at the PPBs, which enhanced the bonding between deposited particles, particularly in samples heat treated at high temperatures.

While we have shown that HTs can increase strength and ductility of CS deposits, for most CS repairs, HT of repaired components will not be practical. However, thermal processing of feedstock powders prior to deposition could yield benefits. Also, future applications might arise that involve use of CS in additive manufacturing, and in such cases, post-deposition HT would be viable.

5. ACKNOWLEDGEMENTS

6. REFERENCES

[1] V.K. Champagne, The Cold Spray Materials Deposition Process: Fundamentals and Applications, Woodhead Publishing Limited, Cambridge, 2007.

[2] T. Schmidt, F. Gärtner, H. Assadi, H. Kreye, Acta Mater. 54 (2006) 729–742.

[3] M.R. Rokni, C.A. Widener, G.A. Crawford, Surf. Coat. Technol. 251 (2014) 254-263.

[4] M.R. Rokni, C.A. Widener, V.R. Champagne, J. Thermal Spray Technol. 23 (2014) 514-524.

[5] D. Poirier, J-G. Legoux, R.A. Drew, R. Gauvin, J. Thermal Spray Technol. 20 (2011) 275-284.

[6] M.R. Rokni, C.A. Widener, G.A. Crawford, M.K. West, Mater. Sci. Eng. A 625 (2015) 19-27.

[7] E. Irissou, J-G. Legoux, A. Ryabinin, B. Jodoin, C. Moreau, J. Thermal Spray Technol. 17 (2008) 495-516.

[8] H. Singh, T.S. Sidhu, S.B.S. Kalsi, Fracture and Structural Integrity, 22 (2012) 69-84.

[9] M.R. Rokni, C.A. Widener, S.P. Ahrenkiel, B.K. Jasthi, V.R. Champagne, Surf. Eng. 30 (2014) 361-368.

[10] S.H. Zahiri, D. Fraser, M. Jahedi, J. Thermal Spray Technol. 18 (2009) 16-22.

[11] Y. Zou, D. Goldbaum, J.A. Szpunar, S. Yue, Scripta Mater. 62 (2010) 395–398.

[12] Y. Zou, W. Qin, E. Irissou, J-G. Legoux, S. Yue, and Jerzy A. Szpunar. Scr. Mater. 61 (2009) 899–902.

[13] M.R. Rokni, C.A. Widener, V.R. Champagne, Appl. Surf. Sci. 290 (2014) 482-489.

[14] R.Z. Valiev, Y. Estrin, Z. Horita, T.G. Langdon, M.J. Zechetbauer, Y.T. Zhu, Jom 58 (2006) 33-39.

[15] J. Jiang, Y. Ding, F. Zuo, A. Shan, Scr. Mater. 60 (2009) 905–908.

[16] M.R. Rokni, C.A. Widener, A.T. Nardi, V.K. Champagne, Appl. Surf. Sci. 305 (2014) 797-804.

[17] Y.H. Zhao, X.Z. Liao, Z. Jin, R.Z. Valiev, Y.T. Zhu, Acta Mater. 52 (2004) 4589-4599.

[18] W.J. Kim, C.S. Chung, D.S. Ma, S.I. Hong, H.K. Kim, Scr. Mater. 49 (2003) 333-338.

[19] Z. Horita, K. Ohashi, T. Fujita, K. Kaneko, T.G. Langdon, Adv. Mater. 17 (2005) 1599-1602.

[20] Y.H. Zhao, X.Z. Liao, S. Cheng, E. Ma, Y.T. Zhu, Adv. Mater. 18 (2006) 2280-2283.

[21] W.J. Kim, J.K. Kim, H.K. Kim, J.W. Park, Y.H. Jeong, J. Alloys Compd. 450 (2008) 222-228.

[22] Y.H. Zhao, X.Z. Liao, Z. Jin, R.Z. Valiev, Y.T. Zhu, Acta Mater. 52 (2004) 4589-4599.

[23] M.J. Starink, S.C. Wang, Acta Mater. 51 (2003) 5131–5150.

[24] M.H. Li, Y.Q. Yang, Z.Q. Feng, G.H. Feng, B. Huang, Y.X. Chen, M. Han, J.G. Ru, Intermetallics 55 (2014) 49-55.

[25] M.J. Starink, X.M. Li, Metall. Mater. Trans. A 34 (2003) 899–911.

[26] E. Calla, D.G. McCartney, P.H. Shipway, J. Thermal Spray Technol. 15 (2006) 255-262.

[27] A.C. Hall, D.J. Cook, R.A. Neiser, T.J. Roemer, D.A. Hirschfeld, J. Thermal Spray Technol. 15 (2006) 233-238.

[28] R. Huang, M. Sone, W. Ma, H. Fukanuma, Surf. Coat. Technol. 261 (2015) 278–288.

[29] W.Y. Li, X.P. Guo, C. Verdy, L. Dembinski, H.L. Liao, C. Coddet, Scr. Mater. 55 (2006) 327-330.

[30] W.Y. Li, C. Zhang, H. Liao, C. Coddet, J. Coat. Technol. Res. 6 (2009) 401–406.

[31] X-M. Meng, J-B. Zhang, W. Han, J. Zhao, Y-L. Liang, Appl. Surf. Sci. 258 (2011) 700-704.

[32] M.R. Rokni, C.A. Widener, V.K. Champagne, G.A. Crawford, Surf. Coat. Technol. 276 (2015) 305-315.

[33] M.R. Rokni, A. Zarei-Hanzaki, A.A. Roostaei, A. Abolhasani, Mater. Des. 32 (2011) 4955-4960.

[34] M.R. Rokni, A. Zarei-Hanzaki, A.A. Roostaei, H.R. Abedi, Mater. Des. 32 (2011) 2339-2344.

[35] ASM Committee on Gas Carburizing, Carbonitriding, and Nitriding, Gas Nitriding, Heat Treatment: ASM Handbook, 4, American Society of Metals, Materials Park, OH, (1991) 191.

[36] L.P. Troeger, Jr. E.A. Starke, Mater. Sci. Eng. A 293 (2000) 19–29.

[37] J.J. Hoyt, Acta Metall. 39 (1991) 2091-2098.

[38] M.R. Rokni, A. Zarei-Hanzaki, H.R. Abedi, Mater. Sci. Eng. A 532 (2012) 593-600.

[39] F.J. Humphreys, M. Hatherly, Recrystallization and Related Annealing Phenomena, 2nd edition, Pergamon Press, Oxford, 2004.